Influence of Doppler Bin Width on GNSS Detection Probabilities

Bernhard C. Geiger, *Student Member, IEEE* and Christian Vogel *Senior Member, IEEE*

***Abstract*—The acquisition stage in GNSS receivers determines Doppler shifts and code phases of visible satellites. Acquisition is thus a search in two continuous dimensions, where the digital algorithms require a partitioning of the search space into cells.**

We present analytic expressions for the acquisition performance depending on the partitioning of the Doppler frequency domain. In particular, the impact of the number and width of Doppler bins is analyzed. The presented results are verified by simulations.

***Index Terms*—GNSS, acquisition, Doppler bin width, receiver operating characteristics**

I. Introduction

In Global Navigation Satellite Systems (GNSS) every satellite is transmitting a particular pseudo-random noise (PRN) code, which is known at the receiver. Satellites are acquired by correlating the received signal and local code signals and comparing the results against a threshold. In practice, the local replica of the transmitted code signal differs from the received code signal by a code phase shift (i.e., time lag) and a Doppler shift. Both have to be determined simultaneously in a two-dimensional search. The results of this search, which is usually called acquisition, are required for presetting subsequent stages of the GNSS receiver.

For this two-dimensional search, the continuous time-frequency uncertainty region is divided into cells, each corresponding to a particular Doppler frequency and a particular code phase. Typically, the number of considered code phases is predetermined by the sampling rate and optional decimation/interpolation methods, whereas the width (and, thus, the number) of Doppler bins is only limited by the effective bandwidth of subsequent signal processing stages [1]. In many civil GNSS receivers exploiting the GPS L1 C/A code [2], the integration period of the correlator is set to the code period of 1 ms. The corresponding Doppler bin widths range from 500 to 667 Hz (see [3]–[5] as well as [6] and the references therein). Unsurprisingly, the choice of the Doppler bin width strongly influences the acquisition performance: Not only that the Doppler bin width is inversely proportional to the number of cells to be searched, it also strongly influences the probability of signal detection. Aside from that, the probability of false positive detections at a Doppler bin adjacent to the correct one increases for small Doppler bins.

Bernhard C. Geiger is with the Signal Processing and Speech Communication Laboratory, Graz University of Technology, A-8010 Graz, Austria (email: geiger@tugraz.at).

Christian Vogel is with the Telecommunications Research Center Vienna (FTW), A-1220 Vienna, Austria (email: c.vogel@ieee.org).

Non-coherent acquisition methods take the squared magnitude of the correlation coefficients as a decision metric to overcome unknown carrier phases and possible data modulation. For these methods, the computation of the receiver operating characteristics is a well-investigated field of research. The literature provides detection and false alarm probabilities for single cells [5], a serial search over all cells with threshold comparison [7], [8], a maximum search [9], [10] and combinations thereof [11]. In [12], a comparison of the abovementioned techniques is provided for an L1 GPS receiver. Detection probabilities for an L5 GPS receiver with different algorithms combining data and pilot signals are considered in [13], from which the comprehensive signal model was largely adopted in this work. In [12], both the number of Doppler bins and side lobes resulting from adjacent Doppler bins are considered; the latter are only obtained by means of simulations. Analytical results for the effect of residual Doppler shifts on the acquisition performance have been presented in [14]. There, also the effect of a single adjacent Doppler bin containing significant energy was analyzed, however, a detection in either of these bins was considered correct and detection performance was evaluated only numerically. All these works, however, are lacking an analysis of the influence of the Doppler bin width on detection performance in terms of closed-form expressions.

In this work, we fill this gap by deriving expressions for cell detection probabilities as a function of the Doppler bin width. These cell probabilities are then used to compute global detection and false alarm probabilities, which further depend on the number of Doppler bins. With the help of this theoretical framework, a proper analysis and, maybe even more importantly, a performance-oriented design of GNSS acquisition stages is possible. Moreover, while the focus of this work is on GNSS receivers, the results can be applied to other CDMA systems affected by large Doppler shifts.

The remainder of this article is organized as follows: In Section II the signal model is introduced, while Section III gives a detailed analysis of the acquisition process. The main contribution of this work is concentrated in Sections IV and V: The former is devoted to deriving global detection and false alarm probabilities for generalized cell probabilities, while in the latter the influence of the Doppler bin width on cell detection probabilities is discussed. The analytic results are finally verified by extensive simulations in Section VI.

II. Signal Model

After front-end filtering, downconversion to the intermediate frequency (IF), and A/D conversion, the signal received from

a single satellite can be represented as [12]

$$r_{IF}[n] = \sqrt{2C}\, y[n] \cos\Big[(\theta_{IF} + \theta_D)\, n - \vartheta\Big] + \eta[n] \quad (1)$$

where C is the signal power, $\theta_{IF} = \frac{2\pi f_{IF}}{f_s}$ and $\theta_D = \frac{2\pi f_D}{f_s}$ are the sampled angular equivalents of the intermediate and Doppler frequencies f_{IF} and f_D, respectively, and ϑ is a phase shift introduced by the transmission and the noncoherent downconversion to IF. If the ideal front-end filter has a bandwidth equal to $\frac{f_s}{2}$ with f_s being the sampling frequency, the noise signal $\eta[n]$ is assumed to be Gaussian with variance [15, pp. 556, Prop. 25.15.2]

$$\sigma_\eta^2 = \frac{N_0 f_s}{2} \quad (2)$$

and with an autocorrelation function of [13]

$$R_{\eta,\eta}[m] = \mathrm{E}\left\{\eta[n]\eta[n-m]\right\} = \sigma_\eta^2 \delta[m]. \quad (3)$$

In these equations, $\frac{N_0}{2}$ is the two-sided noise power spectral density. The carrier is modulated by

$$y[n] = d[n]c[n] \quad (4)$$

where $d[n]$ is the data message and $c[n]$ is the binary PRN code, i.e., $c[n] = \pm 1$. For the sake of simplicity, this work only considers the GPS L1 C/A code with a number of chips per code period $N_C = 1023$ and a code period $T_{per} = 1$ ms [5]. Furthermore, it is assumed that no data is modulated on the PRN code, i.e., $d[n] = 1$. This assumption is unproblematic for the GPS L1 C/A codes, since the 20 ms duration of a data bit is significantly larger than the code period. If acquisition is performed twice for two consecutive C/A code periods and by taking the result with the stronger correlation peak, it can be guaranteed that no bit transition occurs within the considered code period [3]. For modern codes, where the code period is equal to the bit duration (e.g., the GPS L2 CM code) the effects of bit transitions can be mitigated using non-coherent integration [16] or aided acquisition [17].

III. Acquisition System

As stated in the introduction, the continuous time-frequency uncertainty region has to be partitioned into cells to make acquisition tractable. Let us, for the remainder of this work, assume that the partitioning of the frequency domain is uniform, and that each of the K resulting Doppler bins has a width W, as shown in Fig. 1. Given a maximum expected Doppler frequency $\pm f_{D,\max}$, the number of bins, K, is given as

$$K = \frac{2 f_{D,\max}}{W}. \quad (5)$$

In the acquisition process illustrated in Fig. 2, the received signal $r_{IF}[n]$ is first downconverted using an expected Doppler frequency $\theta_{\hat{k}}$. The obtained signal $r_B[n]$ can be described utilizing (1) by

$$\begin{aligned} r_B[n] &= r_{IF}[n] e^{\jmath(\theta_{\hat{k}} + \theta_{IF})n} \quad (6)\\ &= \sqrt{\frac{C}{2}} y[n] \left(e^{\jmath(2\theta_{IF} + \Sigma\theta_{\hat{k}})n - \jmath\vartheta} + e^{\jmath\Delta\theta_{\hat{k}} n + \jmath\vartheta}\right)\\ &\quad + \tilde{\eta}[n] \quad (7) \end{aligned}$$

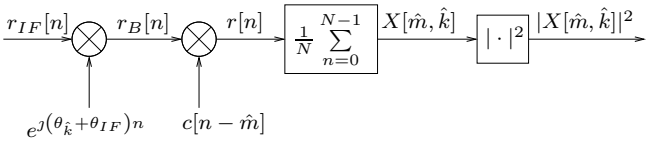

Fig. 2. Acquisition of a signal with unknown Doppler frequency and code phase.

with $\Delta\theta_{\hat{k}} = \theta_{\hat{k}} - \theta_D$ and $\Sigma\theta_{\hat{k}} = \theta_{\hat{k}} + \theta_D$. The noise signal $\tilde{\eta}[n]$ is a zero-mean circular-symmetric complex Gaussian (ZMCSCG) signal with variances $\frac{\sigma_\eta^2}{2}$ for real and imaginary parts. After downconversion the signal is multiplied with the spreading code using an expected code phase $\hat{m}$. Thus,

$$\begin{aligned} r[n] &= r_B[n] c[n-\hat{m}] \quad (8)\\ &= \sqrt{\frac{C}{2}} y[n] c[n-\hat{m}] \left(e^{\jmath(2\theta_{IF} + \Sigma\theta_{\hat{k}})n - \jmath\vartheta} + e^{\jmath\Delta\theta_{\hat{k}} n + \jmath\vartheta}\right)\\ &\quad + \tilde{\eta}[n] c[n-\hat{m}] \quad (9) \end{aligned}$$

where $c[n-\hat{m}]$ is the code $c[n]$ circularly shifted by $\hat{m}$. The decision metric $X[\hat{m},\hat{k}]$ is obtained by averaging the signal over one code period T_{per},

$$X[\hat{m},\hat{k}] = \frac{1}{N}\sum_{n=0}^{N-1} r[n] \quad (10)$$

where the number of samples within one code period is given by

$$N = T_{per} f_s. \quad (11)$$

In this operation, the high-frequency term $e^{\jmath(2\theta_{IF} + \Sigma\theta_{\hat{k}})n - \jmath\vartheta}$ vanishes and the bounded sum over the low-frequency term can be represented by a Dirichlet kernel:

$$\frac{1}{N}\sum_{n=0}^{N-1} e^{\jmath\Delta\theta_{\hat{k}} n} = e^{\jmath\Delta\theta_{\hat{k}}\frac{N-1}{2}} \frac{\sin\left(\frac{\Delta\theta_{\hat{k}}}{2}N\right)}{N\sin\left(\frac{\Delta\theta_{\hat{k}}}{2}\right)} \quad (12)$$

Following the reasoning in [18], the influences of time lags and Doppler frequencies can be separated on average. This argument is supported by extensive simulations showing that the error resulting from this approximation is well below maximum side lobe levels (-21 dB according to [5]) and can thus be neglected. We therefore get for the decision metric:

$$X[\hat{m},\hat{k}] = e^{\jmath\Delta\theta_{\hat{k}}\frac{N-1}{2} + \jmath\vartheta} \frac{\sin\left(\frac{\Delta\theta_{\hat{k}}}{2}N\right)}{N\sin\left(\frac{\Delta\theta_{\hat{k}}}{2}\right)} \sqrt{\frac{C}{2}} R_{y,c}[\hat{m}] + n[\hat{m}] \quad (13)$$

where $R_{y,c}[\hat{m}]$ is the correlation function between $y[n]$ and the local code $c[n]$ evaluated at lag $\hat{m}$. The noise signal $n[\hat{m}]$ is the average of N independent ZMCSCG samples, thus the variances of the real and imaginary parts reduce with (11) to

$$\frac{\sigma_n^2}{2} = \frac{\sigma_\eta^2}{2N} = \frac{N_0 f_s}{4N} = \frac{N_0}{4T_{per}}. \quad (14)$$

Note that the spreading code $c[n]$ has to be upsampled to the sampling rate f_s prior to correlation. Depending on the implementation of the correlation (matched filter, parallel code phase search [3], etc.) samples of the decision metric adjacent

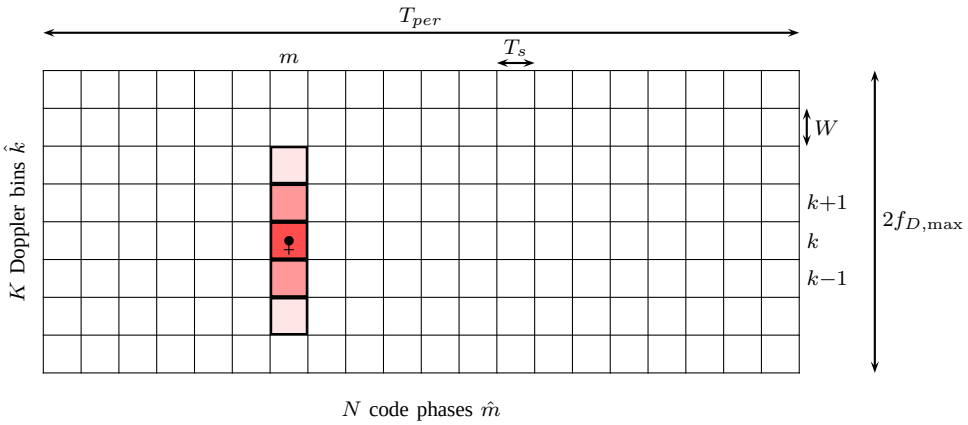

Fig. 1. Partitioning of the continuous time-frequency uncertainty region. The correct code phase is denoted by m, the correct Doppler bin by k. The plus-sign indicates the true Doppler frequency θ_D, the dot shows the Doppler estimate θ_k minimizing the residual Doppler difference $\Delta\theta_{\hat{k}}$. Note that adjacent Doppler bins can contain significant signal energy (indicated by different shading; cf. Sections IV and V).

in the code phase domain are not necessarily statistically independent: The correlation function can, e.g., be computed for all lags $\hat{m}$ and a particular Doppler estimate $\hat{k}$ based on the same set of N input samples. In this case the correlation sum runs over differently weighted moving average filtered input samples, where the weights are ± 1 and the filter order is identical to the upsampling factor $\frac{N}{N_C}$ [19]. This dependence can be exploited to significantly reduce the computational complexity of the correlation process by means of averaging correlation [20], [21]. The result of this averaging correlation is not only a decimation of the correlation function from sampling rate to chip rate (i.e., $N = N_C$), but also yields statistical independence of samples adjacent in the code phase domain.

The decision is finally based on the squared magnitude of the decision metric $X[\hat{m}, \hat{k}]$,

$$|X[\hat{m}, \hat{k}]|^2 = \Re\{X[\hat{m}, \hat{k}]\}^2 + \Im\{X[\hat{m}, \hat{k}]\}^2, \tag{15}$$

which follows for given $\hat{m}$ and $\theta_{\hat{k}}$ a non-central χ^2-distribution with two degrees of freedom and the non-centrality parameter

$$L_{\hat{m},\hat{k}} = \frac{\mathrm{E}\left\{\Re\{X[\hat{m}, \hat{k}]\}\right\}^2}{\frac{\sigma_n^2}{2}} + \frac{\mathrm{E}\left\{\Im\{X[\hat{m}, \hat{k}]\}\right\}^2}{\frac{\sigma_n^2}{2}} \tag{16}$$

$$= 2T_{per}\frac{C}{N_0}\frac{\sin^2\left(\frac{\Delta\theta_{\hat{k}}}{2}N\right)}{N^2\sin^2\left(\frac{\Delta\theta_{\hat{k}}}{2}\right)}R_{y,c}^2[\hat{m}]. \tag{17}$$

Note that the squared means have to be normalized by the corresponding variances, since the χ^2-distribution is defined as the sum of squares of Gaussian random variables with unit variance [22, pp. 940]. With

$$\Delta\theta_{\hat{k}} = 2\pi\frac{\Delta f_{\hat{k}}}{f_s} = 2\pi\Delta f_{\hat{k}}\frac{T_{per}}{N}, \tag{18}$$

and due to the fact that the maximum Doppler difference $\Delta f_{\hat{k}}$ is in the order of a few kHz, even for $N = N_C = 1023$ the Dirichlet kernel can be well approximated by a sinc kernel. Using $\mathrm{sinc}(x) = \frac{\sin(\pi x)}{\pi x}$ this finally leads to

$$L_{\hat{m},\hat{k}} = 2T_{per}\frac{C}{N_0}\mathrm{sinc}^2\left(\Delta f_{\hat{k}}T_{per}\right)R_{y,c}^2[\hat{m}]. \tag{19}$$

IV. Detection Probabilities

We define a *global detection* as the event that the cell selected by the employed search strategy is the correct cell, i.e., the one with the correct code phase $\hat{m} = m$ and with the correct Doppler index

$$\hat{k} = k = \arg\min_{\tilde{k}}\left\{|\theta_D - \theta_{\tilde{k}}|\right\}. \tag{20}$$

If a cell is chosen in the absence of a signal, we will call this event a *global false alarm*. If the search algorithm chooses no cell at all or the wrong cell in the presence of a signal, neither a false alarm nor a detection occurs. We will limit ourselves to search strategies employing threshold comparison, i.e., a cell detection or cell false alarm is triggered whenever the decision metric $|X[\hat{m}, \hat{k}]|^2$ for this cell exceeds a certain threshold β. A decision based on the ratio between the largest and the second largest value of $|X[\hat{m}, \hat{k}]|^2$ of a subset of cells was suggested by [23], [24] after the introduction of this ratio as a reliability measure in [17]. However, the performance of this method has been analyzed just recently [25], and it was shown that a decision based on threshold comparison outperforms the ratio detector [26].

On one hand, as it can be seen from (19), the non-centrality parameter $L_{\hat{m},\hat{k}}$ of the χ^2-distribution is maximized for the correct code phase m and the correct Doppler bin k. On the other hand, whenever the desired satellite PRN code sequence is not contained in the received signal, whenever the difference between the actual and the estimated Doppler frequencies is too large, or whenever the code phase is not correct ($\hat{m} \neq m$), the non-centrality parameter $L_{\hat{m},\hat{k}} \approx 0$, neglecting side lobe and cross-correlation levels. Assuming $L_{\hat{m},\hat{k}} = 0$ immediately translates to the fact that the χ^2-distribution changes from a non-central to a central distribution.

In this Section, we will derive general relations between the cell and the global detection and false alarm probabilities. In particular, we consider not only the number K of Doppler bins, but also take into account that cells with correct code phases, but wrong Doppler indices, may have a non-centrality parameter $L_{\hat{m},\hat{k}} > 0$.

A. Cell Detection Probabilities

Let us define the *cell false alarm* as the decision metric $|X[\hat{m},\hat{k}]|^2$ exceeding a certain threshold β given that $L_{\hat{m},\hat{k}} = 0$. Then, the cell false alarm probability becomes

$$P_{fa}(\beta) = \text{Prob}\left(|X[\hat{m},\hat{k}]|^2 > \beta \mid L_{\hat{m},\hat{k}} = 0\right) \tag{21}$$

which for a central χ^2-distribution is equivalent to [10]

$$P_{fa}(\beta) = e^{-\frac{\beta}{2\sigma_n^2}}. \tag{22}$$

Conversely, whenever the decision metric exceeds the threshold for a non-central χ^2-distribution ($L_{\hat{m},\hat{k}} > 0$), we will call this event a *cell detection*. Thus, the cell detection probability is

$$\begin{aligned} P_{det}(\beta, L_{\hat{m},\hat{k}}) &= \text{Prob}\left(|X[\hat{m},\hat{k}]|^2 > \beta \mid L_{\hat{m},\hat{k}} > 0\right) \\ &= \text{Q}_1\left(\sqrt{L_{\hat{m},\hat{k}}}, \sqrt{\frac{\beta}{\sigma_n^2}}\right) \end{aligned} \tag{23}$$

where $\text{Q}_1(\cdot,\cdot)$ is the Marcum Q-function [27], [28]. Note that in fact $P_{fa}(\beta)$ is a special case of $P_{det}(\beta, L_{\hat{m},\hat{k}})$, namely for $L_{\hat{m},\hat{k}} = 0$.

B. Global Detection Probabilities – Naive Assumption

Let us now assume that the acquisition is implemented as a serial search over the two-dimensional uncertainty region comprised of NK cells, and the search is stopped when $|X[\hat{m},\hat{k}]|^2$ exceeds the threshold β for the first time. Furthermore, it is assumed that there is only one cell containing significant signal energy, i.e., there is only one ($\hat{m}$, $\hat{k}$)-pair for which the decision metric $|X[\hat{m},\hat{k}]|^2$ is non-centrally χ^2-distributed – namely the pair (m, k). We will call the event of a threshold crossing a global false alarm whenever the desired PRN code is not contained in the received signal. A global detection, as already mentioned, denotes the event when the first threshold crossing in the serial search occurs at the correct code phase m and the correct Doppler bin k. Following [12], the global false alarm probability $P_{FA}(\beta)$ therefore calculates to

$$P_{FA}(\beta) = 1 - (1 - P_{fa}(\beta))^{NK}, \tag{24}$$

whereas the global detection probability $P_{DET}(\beta)$ can be calculated as

$$P_{DET}(\beta) = \frac{1}{NK}\frac{1-(1-P_{fa}(\beta))^{NK}}{P_{fa}(\beta)} P_{det}(\beta, L_{m,k}). \tag{25}$$

For very small values of $P_{fa}(\beta)$ the above equations can be approximated by $P_{FA}(\beta) \approx NKP_{fa}(\beta)$ and $P_{DET}(\beta) \approx P_{det}(\beta)$ [12].

The assumption of a single signal cell (i.e., a cell for which $L_{\hat{m},\hat{k}} > 0$) is clearly a strong one, since the side lobe and cross-correlation levels of the correlation function, a non-zero width of the correlation main lobe for $N > N_c$, and signal energy in Doppler bins adjacent to the correct one will lead to $L_{\hat{m},\hat{k}} > 0$ for more than one cell. Effects of side lobes and cross-correlations in the code phase search can be neglected in medium SNR levels or mitigated by appropriate threshold settings, and the effects due to the correlation main lobe can be reduced by means of averaging correlation [19]–[21]. Signal energy in adjacent Doppler bins, however, not only affects global detection probabilities, but also depends on the width of the Doppler bins. A proper analysis of this influence can not be found in the literature.

C. Global Detection Probabilities – Refined Model

In accordance with what has been said, let $L_{m,k}$ be the non-centrality parameter of the correct cell, and let $L_{m,k\pm1}$, $L_{m,k\pm2}$, etc. denote the non-centrality parameters of cells with the correct code phase m, but for the first, second, etc. adjacent Doppler bins. For all other code phases let $L_{\hat{m},\hat{k}} = 0$ (in the absence of the desired PRN code let $L_{\hat{m},\hat{k}} = 0$ for all cells). In other words, each Doppler bin $\hat{k}$ contains at most one signal cell at the correct code phase m (see Fig. 1) with an expected non-centrality parameter $L_{m,\hat{k}}$. Again, acquisition is assumed to take place as a serial search with threshold comparison. It is important to note that increased detection probabilities for wrong Doppler bins are adverse in terms of global detection probabilities.

Since there is now more than a single signal cell, the direction of the serial search has an influence on the global detection probability. In other words, searching all code phases for each Doppler bin and searching all Doppler bins for each code phase leads to different performance results. Note that both methods can be efficiently implemented using the FFT: In this case, the former option is called parallel code phase search, while the latter is often referred to as parallel frequency search [3]. Following the reasoning in [12], the probability of detection for a search over all code phases for each Doppler bin can be calculated as

$$\begin{aligned} P_{DET}(\beta) = \frac{P_{det}(\beta, L_{m,k})}{KN}\frac{1-\overline{P}_{fa}^{N}(\beta)}{P_{fa}(\beta)} \\ \times \left[1 + \sum_{n=1}^{K-1}\overline{P}_{fa}^{n(N-1)}(\beta)\prod_{l=1}^{n}\overline{P}_{det}(\beta, L_{m,k-l})\right] \end{aligned} \tag{26}$$

where $\overline{P}_{fa}(\beta) = 1 - P_{fa}(\beta)$ and $\overline{P}_{det}(\beta, L_{m,\hat{k}}) = 1 - P_{det}(\beta, L_{m,\hat{k}})$. The probability of detection for a search over all Doppler bins for each code phase calculates to

$$\begin{aligned} P_{DET}(\beta) = \frac{P_{det}(\beta, L_{m,k})}{KN}\left(1 + \sum_{n=1}^{K-1}\prod_{l=1}^{n}\overline{P}_{det}(\beta, L_{m,k-l})\right) \\ \times \frac{1-\overline{P}_{fa}^{KN}(\beta)}{1-\overline{P}_{fa}^{K}(\beta)}. \end{aligned} \tag{27}$$

Although theoretically different, for small cell false alarm probabilities $P_{fa}(\beta)$ we can write $\overline{P}_{fa}^{M} \approx 1 - MP_{fa}(\beta) \approx 1$ and thus obtain as an approximation for both search directions:

$$P_{DET}(\beta) = \frac{P_{det}(\beta, L_{m,k})}{K}\left(1 + \sum_{n=1}^{K-1}\prod_{l=1}^{n}\overline{P}_{det}(\beta, L_{m,k-l})\right) \tag{28}$$

Depending on the acquisition strategy, this approximation can be shown to hold for a wide range of SNR. This is due to

setting the threshold to obtain a constant false alarm rate [5], which can be done efficiently by continuously measuring the noise floor [26].

It is worth mentioning that the global false alarm probability is the same for the naive and the refined model, i.e., it is always given by (24). Further, when the naive assumption holds, i.e., $L_{\hat{m},\hat{k}} = 0$ for $\hat{m} \neq m$ and $\hat{k} \neq k$, both (26) and (27) reduce to (25), while the same does not hold for the approximation (28). Finally, both the naive and the refined model assume that the correct cell is uniformly distributed over the two-dimensional search space. While this assumption can be justified for the code phase domain, depending on the approximate time and position of the receiver, an estimated Doppler frequency can be computed, from which the search should be initiated [1]. Since the Doppler frequency is likely close to its estimate if the estimation process was successful, the uniformity assumption is too restrictive and the obtained results underestimate the detection performance of the receiver.

V. Influence of Doppler Bin Width on the Decision Metric

We have defined the non-centrality parameter of the χ^2-distribution modeling the decision metric $|X[\hat{m},\hat{k}]|^2$ in (19), which shows that it is proportional to the squared sinc of the Doppler difference $\Delta f_{\hat{k}} = f_{\hat{k}} - f_D$, as well as to the squared correlation function $R^2_{y,c}[\hat{m}]$. Using proper decimation methods [19]–[21] and neglecting side lobes and cross-correlation levels we assume that there exists only one single code phase m for which the correlation function is non-zero, and that for this phase we have $R^2_{y,c}[m] = 1$. In the literature (e.g., [9], [13]), however, even the squared sinc is often approximated by unity for the correct Doppler bin, and by zero for all other bins such that

$$L_{m,k} = L_{\max} = 2T_{per}\frac{C}{N_0} \tag{29}$$

$$L_{m,\hat{k}} = 0 \quad \forall \hat{k} \neq k. \tag{30}$$

As Fig. 3 shows, this simplification is too optimistic: For small Doppler bins, such as $W = 200$ Hz, the Doppler bin adjacent to the correct one (the area between the two leftmost dot-markers) has a significant non-centrality parameter $L_{m,k\pm1}$. Moreover, for large Doppler bins (e.g., $W = 700$ Hz) the non-centrality parameter $L_{m,k}$ of the correct Doppler bin might be as low as indicated by the leftmost cross-marker. This Section is thus devoted to a more in-depth analysis of the influence of Doppler bin widths, which will lead to a more realistic characterization of the acquisition performance.

As stated in Section III (see Fig. 1), in the acquisition process the whole Doppler domain is divided into bins of equal width W, which are searched in a serial fashion. The center frequency of a bin represents the Doppler estimate $f_{\hat{k}} = \theta_{\hat{k}}\frac{f_s}{2\pi}$ with which the received signal is demodulated. In the Doppler bin corresponding to the correct Doppler frequency, the remaining difference Δf_k is uniformly distributed within that bin, i.e.,

$$\Delta f_k \sim \mathcal{U}\left(-\frac{W}{2}, \frac{W}{2}\right). \tag{31}$$

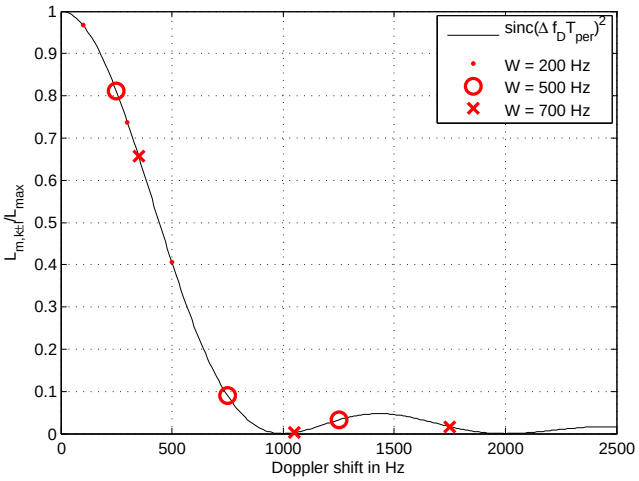

Fig. 3. Squared sinc function for $T_{per} = 1$ ms. Markers indicate Doppler bin boundaries for designated bin widths W.

Further, due to the symmetry of the sinc, for the $k \pm l$-th bin the residual Doppler difference is distributed according to

$$\Delta f_{k\pm l} \sim \mathcal{U}\left((2l-1)\frac{W}{2}, (2l+1)\frac{W}{2}\right) \tag{32}$$

with $l \in \mathbb{N}$. Since now $\Delta f_{\hat{k}}$ is a random variable (RV), also L becomes an RV with probability density function (PDF) $f_L(l)$. The detection probability thus calculates to

$$P_{det}(\beta, L) = \int_{\beta}^{\infty}\int_{-\infty}^{\infty} f_{Y|L}(y|l) f_L(l) dl dy \tag{33}$$

where $f_{Y|L}(y|l)$ is the PDF of $|X[\hat{m},\hat{k}]|^2$ for the cell containing the desired signal conditioned on the non-centrality parameter L. This expression is difficult to compute since the PDF of L is not readily available and also the resulting integrals might not have convenient closed-form solutions. Instead, assuming that the Doppler bins are sufficiently small, it is possible to approximate the PDF of Y to be linearly dependent on L and we get

$$P_{det}(\beta, L) \approx \int_{\beta}^{\infty} f_{Y|L}(y, \mathrm{E}\{L\}) dy, \tag{34}$$

as shown in the Appendix. Exploiting the method for computing the expected value of a function of a random variable from [29, pp. 142] and using the uniform distribution (32), it is straightforward to compute $L_{m,\hat{k}} = L_{m,k\pm l}$

$$L_{m,k\pm l} = 2T_{per}\frac{1}{W}\frac{C}{N_0}\int_{(2l-1)\frac{W}{2}}^{(2l+1)\frac{W}{2}} \mathrm{sinc}^2\left(\Delta f_{\hat{k}} T_{per}\right) d(\Delta f_{\hat{k}}) \tag{35}$$

Substituting $x = \Delta f_{\hat{k}} T_{per}$ we get $dx = T_{per} d(\Delta f_{\hat{k}})$ and

$$L_{m,k\pm l} = \frac{2}{W}\frac{C}{N_0}\int_{\underline{f}_l T_{per}}^{\overline{f}_l T_{per}} \mathrm{sinc}^2(x)\, dx. \tag{36}$$

where $\underline{f}_l = (2l-1)\frac{W}{2}$ and $\overline{f}_l = (2l+1)\frac{W}{2}$ denote the lower and upper frequency bounds of the $k \pm l$-th Doppler bin. We

obtain

$$L_{m,k\pm l} = \frac{2}{W}\frac{C}{N_0}\frac{1}{\pi}\Big[\mathrm{Si}(2\pi\overline{f}_l T_{per}) - \mathrm{Si}(2\pi\underline{f}_l T_{per}) + \frac{\sin^2(\pi\underline{f}_l T_{per})}{\pi\underline{f}_l T_{per}} - \frac{\sin^2(\pi\overline{f}_l T_{per})}{\pi\overline{f}_l T_{per}}\Big] \quad (37)$$

where $\mathrm{Si}(\cdot)$ is the sine integral [22, pp. 231]. For $\underline{f}_l = \overline{f}_l = \frac{W}{2}$ (i.e., for the bin k containing the correct Doppler frequency) this yields

$$L_{m,k} = \frac{2}{W}\frac{C}{N_0}\frac{1}{\pi}\left[2\mathrm{Si}(\pi W T_{per}) - \frac{4\sin^2(\pi\frac{W}{2}T_{per})}{\pi W T_{per}}\right] \quad (38)$$

The sine integral increases monotonously in the interval $[-\pi, \pi]$ and oscillates around the constants $\frac{\pi}{2}$ for positive and around $-\frac{\pi}{2}$ for negative arguments in a decaying manner. Thus, the difference of the sine integrals in (37) will contribute significantly whenever at least one of the arguments falls within $[-\pi, \pi]$, i.e., for low values of $l = |\hat{k} - k|$. Thus, one can expect that Doppler bins close to the correct bin have, on average, large non-centrality parameters, while large offsets lead to small non-centrality parameters. These mathematical considerations are in line with intuition, which suggests that the correct Doppler bin contains most of the energy. Moreover, since for small values of W more bin boundaries may fall in the interval $[-\pi, \pi]$, the correct Doppler bin k on average contains more energy if the bin is small. For large bins the correct Doppler frequency may be far from the bin center, compared to the former case.

While all this reasoning suggests that smaller Doppler bins are preferable, another aspect has to be taken into account: Given a fixed Doppler search range of $\pm f_{D,\max}$, according to (5) K bins have to be searched. Since K is inversely proportional to the bin width W, smaller widths lead to a higher number of bins, which increases the probability of false alarms according to (24) and, consequently, decreases the probability of detection (see (25) and (28)). Moreover, in cases where W is small, bins adjacent to the correct Doppler bin may contain significant signal energy (large $L_{m,k\pm1}$, $L_{m,k\pm2}$, etc.), which can trigger a false detection and thus degrade receiver performance. As a consequence, depending on the threshold and the SNR, there will be an optimal Doppler bin width W maximizing the global detection probability $P_{DET}(\beta)$.

VI. Simulations and Results

To verify the analytic results, a series of simulations was conducted. To this end, a set of satellite signals was generated. For simplicity, it was assumed that just a single satellite (GPS L1 C/A PRN code 1, $N_C = 1023$, $T_{per} = 1$ ms) was visible with random Doppler frequency f_D and code phase m (see below). The carrier-over-noise spectral density ratio $\frac{C}{N_0}$ was set to 40 dBHz unless stated otherwise. After sampling the signal with a high sampling frequency, it was assumed that prior to detection the signal was decimated to the code chipping rate by means of averaging correlation (cf. [20], [21]). Thus, $N = N_C = 1023$. This simplification does not affect the validity of the analysis, since with this method the statistical properties of the cells do not change [19]. It was assumed, however, that during decimation the correct code phase m corresponding to $R_{y,c}[m] = 1$ is preserved.

The Doppler frequency was assumed to be uniformly distributed over the whole Doppler range, i.e., $f_D \sim \mathcal{U}(-f_{D,\max}, f_{D,\max})$, where $f_{D,\max} = 5000$ Hz [1]. To make both simulation and analytic comparison tractable, only two Doppler bins adjacent to the correct bin contained signal energy, i.e., $L_{m,k\pm l} = 0$ for $l = 3, 4, \ldots$, which leads to

$$P_{det}(\beta, L_{m,k\pm l}) = P_{fa}(\beta) \quad \forall l = 3, 4, \ldots \quad (39)$$

This simplification holds well for bin widths greater than 300 Hz, as shown in Fig. 3. The Doppler bin widths were varied within $W \in \{200, 500, 700, 1000\}$. The signals were correlated with PRN codes 1 and 5 for the detection and false alarm probabilities, respectively. For each Doppler bin width W and each value of $\frac{C}{N_0}$ a set of 10^5 correlations was performed.

A serial search is implemented: Starting from the first Doppler bin, all possible code phases are searched sequentially until either the threshold is crossed or until the whole Doppler bin is searched. Then, the next Doppler bin is taken into consideration. If the first threshold crossing occurs at the correct code phase in the correct Doppler bin, the signal is assumed to be detected, while any threshold crossing in the absence of a signal triggers a false alarm. For the analytic results for the global detection probability, the accurate expression (26) was used.

A. Influence of Doppler Bin Width on Cell Probabilities

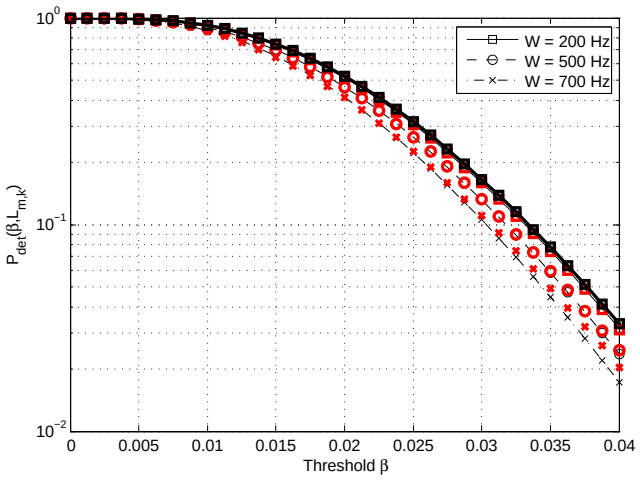

Fig. 4. Cell Detection Probability $P_{det}(\beta, L_{m,k})$ for different Doppler bin widths. Simulated (bold markers) and analytic (lines) results are shown for the correct Doppler bin. The thick solid line indicates $P_{det}(\beta, L_{\max})$.

Figs. 4, 5, and 6 show a comparison between the simulated and analytic cell detection probabilities for the correct, the first, and the second adjacent Doppler bins for different bin widths. It can be seen that there is a good match between the analytic and the simulated results, except for the case of the Doppler bin directly adjacent to the correct one. In this particular case, a separate analysis showed that for $\hat{k} = k \pm 1$ and for larger the Doppler bin widths, (34) is not a good

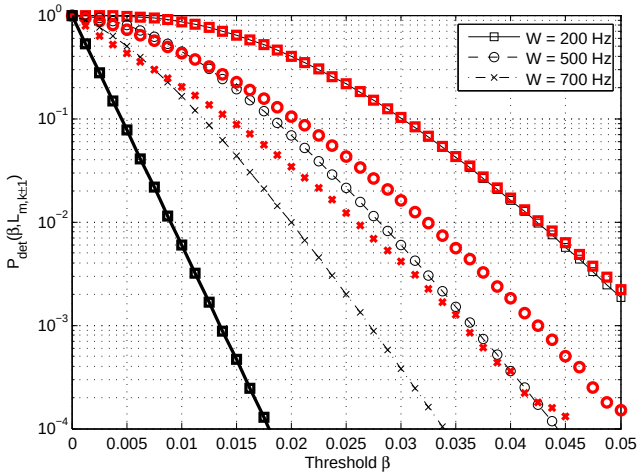

Fig. 5. Cell Detection Probability $P_{det}(\beta, L_{m,k\pm1})$ for different Doppler bin widths. Simulated (bold markers) and analytic (lines) results are shown for the Doppler bin adjacent to the correct one. The thick solid line indicates $P_{det}(\beta, 0) = P_{fa}(\beta)$.

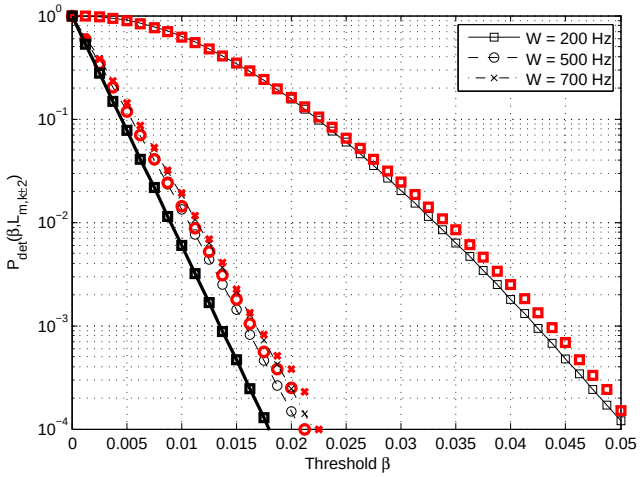

Fig. 6. Cell Detection Probability $P_{det}(\beta, L_{m,k\pm2})$ for different Doppler bin widths. Simulated (bold markers) and analytic (lines) results are shown for the Doppler bin second adjacent to the correct one. The thick solid line indicates $P_{det}(\beta, 0) = P_{fa}(\beta)$.

approximation of (33), which consequently leads to large deviations. This is related to the fact that the linear approximation of the conditional PDF $f_{Y|L}(y, l)$ is not sufficiently accurate for these choices of parameters (see Appendix). Nevertheless, it can be seen that smaller Doppler bins lead to increased cell detection probabilities, both for the correct and adjacent Doppler bins. In addition to that, it is shown (thick lines) that by not considering Doppler bin widths at all, the results would be too optimistic, leading to an overestimation of the global detection probability (see Section VI-B).

The cell false alarm probability does not depend on the noncentrality parameter L, thus it is not affected by the Doppler bin width.

B. Influence of Doppler Bin Width on Global Probabilities

Combining these probabilities to global detection and false alarm probabilities shows another picture: Here, the effect of

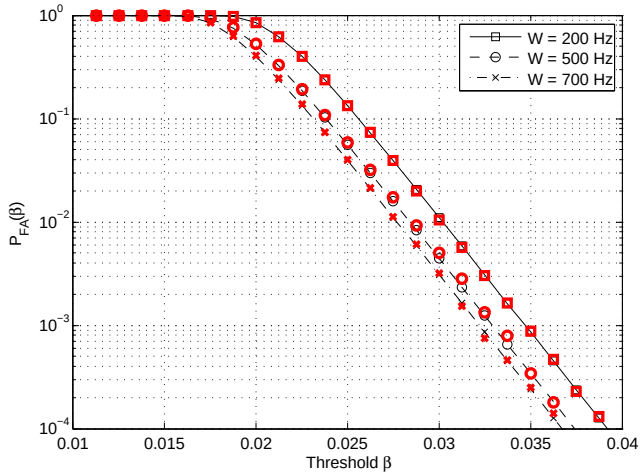

Fig. 7. Global False Alarm Probability $P_{FA}(\beta)$ for different Doppler bin widths. Simulated (bold markers) and analytic (lines) results are shown.

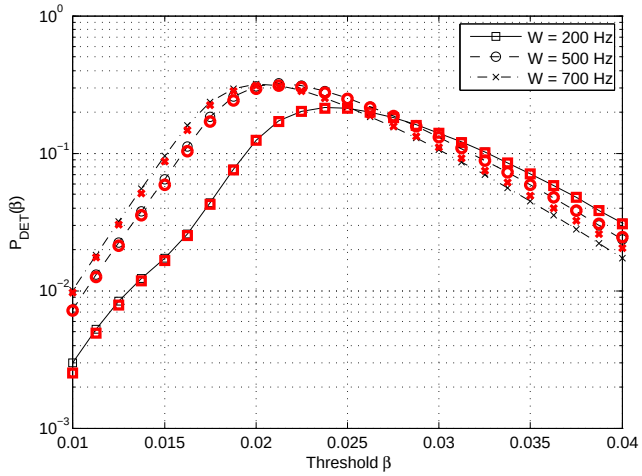

Fig. 8. Global Detection Probability $P_{DET}(\beta)$ for different Doppler bin widths. Simulated (bold markers) and analytic (lines) results are shown.

a greater number of noise cells becomes apparent, showing that smaller Doppler bins do not necessarily lead to improved performance. For example, Fig. 7 shows that the global false alarm probability increases for smaller Doppler bins, i.e., for an increasing number K of bins – this is intuitively understood by looking at (24). Conversely, Fig. 8 shows the probability of detecting the correct cell in a serial search which, especially for small Doppler bins and low thresholds, suffers from high false alarm rates. The additional bend in the curve for $W = 200$ Hz near the maximum is due to significant energy of the adjacent Doppler bins, which increases the probability of triggering a false alarm. As shown, low thresholds benefit from larger Doppler bins (small K, little energy in adjacent bins), whereas the opposite is true for larger values of β. There, small Doppler bins lead to a high $L_{m,k}$, i.e., a high cell detection probability for the correct cell, whereas false alarms are unlikely due to the large threshold.

As Figs. 7 and 8 show, the analytic results are widely validated by the simulations, despite the fact that the detection probability for the Doppler bin with index $k \pm 1$ was

underestimated by the theoretical approximation.

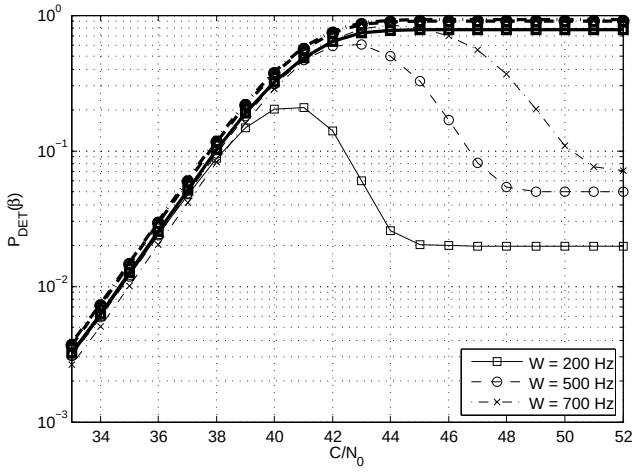

Fig. 9. Global Detection Probability $P_{DET}(\beta)$ for different Doppler bin widths as a function of $\frac{C}{N_0}$. Analytic results are shown for a fixed cell false alarm probability of $P_{fa}(\beta) \approx 10^{-5}$ ($\beta = 0.0225$). Thick lines correspond to $L_{m,k} = L_{\max}$, $L_{m,\hat{k}} = 0$ for all $\hat{k} \neq k$.

Fig. 9 shows the global detection probability for a fixed cell false alarm probability and different values of $\frac{C}{N_0}$. It can be seen that for low values of $\frac{C}{N_0}$ all Doppler bin widths perform almost identically with smaller bins slightly in favor. Differences only become apparent for medium to high values. Fixing the threshold relative to the noise floor has the effect of increasing the probability of a false alarm at an adjacent Doppler bin for large SNR. The detection probability asymptotically approaches the probability that the serial search is started at the correct bin, i.e., $P_{DET}(\beta) = \frac{1}{K}$. Thus, for high SNR and a fixed cell false alarm probability, large Doppler bins perform better than smaller ones.

As one can expect, by neglecting the influence of the Doppler bin width on the cell probabilities, i.e., assuming that there is just one signal cell in the two-dimensional uncertainty region, this behavior cannot be observed. As the thick solid lines in Fig. 9 show, the global detection probability just depends on the SNR and on the total number of cells, NK. Thus, for large $\frac{C}{N_0}$, neglecting adjacent Doppler bins leads to optimistic results for the global detection probability $P_{DET}(\beta)$.

Fig. 10 depicts the global detection probability as a function of the Doppler bin width W, again for a fixed cell false alarm probability. It can be seen that small Doppler bins are in favor for low values of $\frac{C}{N_0}$ (see Fig. 9). If the bins are large, too much energy is lost for the correct bin, while the energy from adjacent bins is buried under the noise floor anyway. For high SNR regions and small W, however, false alarms are likely at adjacent Doppler bins. Again, by neglecting the influence of W on the cell detection probabilities, too optimistic results are obtained. As the thick lines in Fig. 10 show, one may be falsely led to the conclusion that the effect of Doppler bin widths is negligible, and that regardless of the SNR the detection performance is better for large Doppler bins (i.e., for small K).

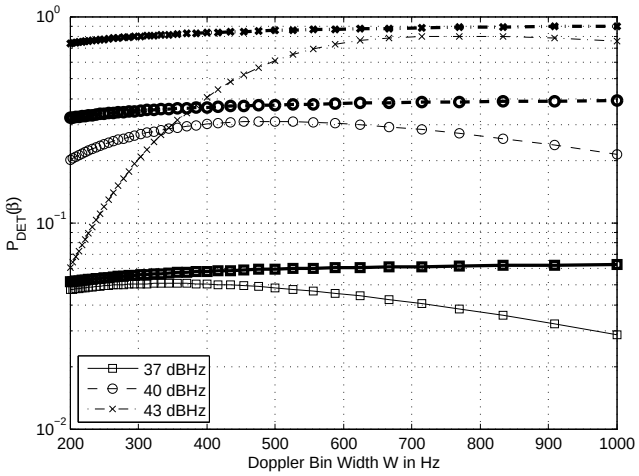

Fig. 10. Global Detection Probability $P_{DET}(\beta)$ for different $\frac{C}{N_0}$ as a function of Doppler bin widths. Analytic results are shown for a fixed cell false alarm probability of $P_{fa}(\beta) \approx 10^{-5}$ ($\beta = 0.0225$). Thick lines correspond to $L_{m,k} = L_{\max}$, $L_{m,\hat{k}} = 0$ for all $\hat{k} \neq k$.

Here, we want to stress that a general statement about the optimal width W and the corresponding number K of the Doppler bins is not possible. The naive assumption of a single signal cell only considers the number K of bins, and thus suggests that few large bins outperform many small ones. This effect of the Doppler bin count K is outweighed by considering the non-centrality parameters of adjacent bins – if the bins are too small, false alarms at adjacent Doppler bins prohibit high detection probabilities. As it turns out, there is a Doppler bin width W optimizing the trade-off. A general statement about this optimum is not possible, since it depends not only on the SNR (cf. Fig. 10), but also on the chosen cell false alarm probability which influences the threshold setting.

C. Receiver Operating Characteristics

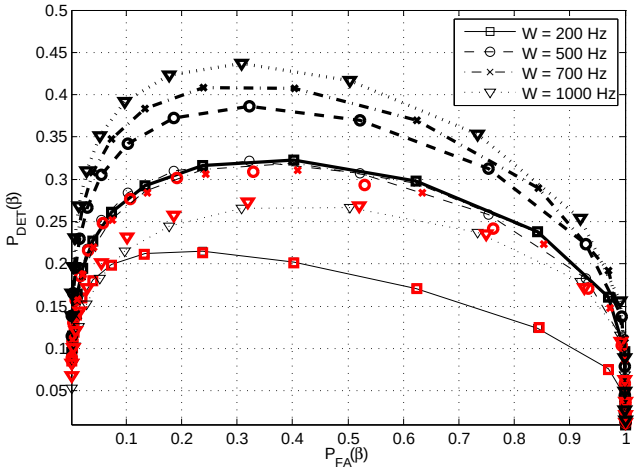

Fig. 11. Receiver Operating Characteristics for $\frac{C}{N_0} = 40$ dBHz. Simulated (red bold markers) and analytic (marked lines) results are compared to the naive assumption of $L_{m,k} = L_{\max}$ and $L_{m,\hat{k}} = 0$ for all $\hat{k} \neq k$ (thick marked line)

Fig. 11 finally plots the global detection probability as a function of the global false alarm probability. Again, it can be seen that analysis and simulation match quite well. As it was expected, neither very small nor very large Doppler bins perform well: In the former case, the false alarm probability is increased, while in the latter the detection probability is decreased. On the other hand, medium Doppler bin widths in the order of 500 to 700 Hz turn out to perform optimally in terms of receiver operating characteristics, at least for this particular value of $\frac{C}{N_0}$.

By neglecting the influence of Doppler bin widths, one again can see that the obtained results are overly optimistic. Looking at the thick lines in Fig. 11, which consider the number of bins, K, but not the influence on the non-centrality parameters $L_{m,\hat{k}}$, one is tempted to conclude that large Doppler bins outperform smaller ones. This result, however, is based entirely on the assumption that there is just one signal cell, and that the energy contained in this cell is independent of the Doppler bin width.

As Fig. 11 shows, despite model inaccuracies pointed out in Section VI-A and in the Appendix, our theoretical framework matches the simulations quite well. In addition to that, compared to the naive assumption of a single signal cell, our model leads to dramatically improved estimates of receiver operating characteristics.

VII. Conclusion

In this article, the influence of Doppler bin widths on GNSS acquisition performance is analyzed. Analytic expressions, linking the Doppler bin width to the detection probabilities, are derived and evaluated. These expressions replace the conventionally used detection and false alarm probabilities, which assume that the search region is populated by noise-only cells except for a single signal cell. This assumption, specifically, is shown to be overly optimistic.

Three different effects of the Doppler bin width are considered: First, the number of bins influencing the total number of cells over which a serial search is conducted. Here it is shown that a large number of bins increases the false alarm probability and decreases the detection probability. Second, the influence of the bin width on the detection probability of the correct cell was analyzed. It turned out that smaller widths improve detection performance significantly. And finally, the influence of the bin widths on the false alarm probability, especially for cells in the close vicinity of the correct cell, where significant signal energy can leak to adjacent Doppler bins was discussed. It was shown that smaller bin widths increase the probability of stopping the search at a wrong Doppler bin, and thus have adverse effects on the detection probability. As a consequence, extreme cases of very small or very large Doppler bins should be avoided when designing the acquisition stage. All these analyses are validated by means of simulations.

Appendix

In this appendix, we show that under a linearity assumption (33) can be approximated by (34). Thus, let us first assume that

$$f_{Y|L}(y,l) \approx (kl+d) f_Y(y, \mathrm{E}\{L\}). \tag{40}$$

Substituting this into (33) leads to

$$\begin{aligned} P_{det}(\beta, L) &= \int_{\beta}^{\infty} \int_{-\infty}^{\infty} f_{Y|L}(y,l) f_L(l) dl dy && (41)\\ &\approx \int_{\beta}^{\infty} \int_{-\infty}^{\infty} (kl+d) f_Y(y, \mathrm{E}\{L\}) f_L(l) dl dy && (42)\\ &= \int_{\beta}^{\infty} f_Y(y, \mathrm{E}\{L\}) \int_{-\infty}^{\infty} (kl+d) f_L(l) dl dy && (43)\\ &= \int_{\beta}^{\infty} f_Y(y, \mathrm{E}\{L\})(k\mathrm{E}\{L\}+d) dy && (44)\\ &= \int_{\beta}^{\infty} f_{Y|L}(y, \mathrm{E}\{L\}) dy, && (45) \end{aligned}$$

which is (34). However, in this equation one needs to make sure that $f_Y(y, \mathrm{E}\{L\})$ depends on the expected value of L such that

$$\int_{-\infty}^{\infty} f_Y(y, \mathrm{E}\{L\})(k\mathrm{E}\{L\}+d) dy = 1 \tag{46}$$

for all $\mathrm{E}\{L\}$. In Fig. 12 this linearity assumption is illustrated. The range between the rightmost marker and the value $L_{m,k\pm l}/L_{\max}$ represents the correct Doppler bin. The range between the two rightmost (leftmost) markers indicate the first (second) adjacent Doppler bin ($k \pm 1$ and $k \pm 2$, respectively; compare to Fig. 3). As it can be seen, both the range between the two leftmost markers and the range between the rightmost marker and the boundary can be well approximated by a line. Thus, (34) approximates (33) well and the corresponding detection probabilities are matching simulations (see Figs. 4 and 6). The range between the two leftmost markers, on the other hand, is only approximately linear for $W = 200$ Hz. For bin widths of $W = 500$ Hz and $W = 700$ Hz the linearity assumption clearly does not hold. As a consequence, the detection probability obtained for the adjacent Doppler bin is valid only for $W = 200$ Hz (see Fig. 5).

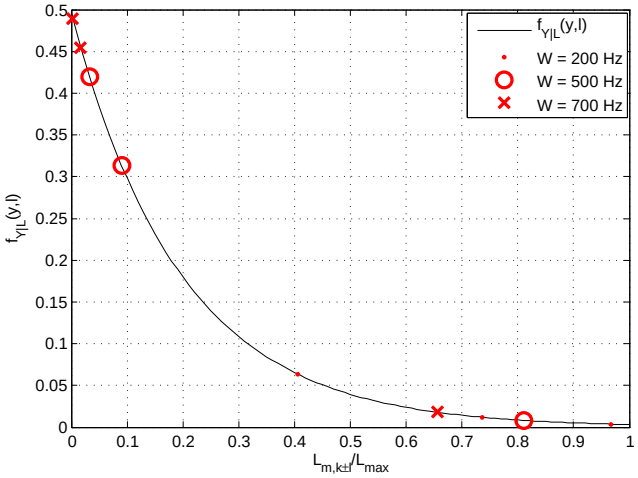

Fig. 12. Conditional probability $f_{Y|L}(y,l)$ evaluated for $T_{per} = 1$ ms, $\frac{C}{N_0} = 40$ dBHz, and $y = 0.0225$. Markers indicate Doppler bin boundaries for designated bin widths W.

ACKNOWLEDGMENTS

The authors would like to thank Daniel Arnitz for valuable suggestions and feel particularly indebted to the anonymous reviewers helping to improve the manuscript. This work was partially funded by the Austrian Research Promotion Agency under the project "SoftGNSS 2", project number 819682.

REFERENCES

[1] M. S. Grewal, L. R. Weill, and A. P. Andrews, *Global Positioning Systems, Inertial Navigation, and Integration*. John Wiley & Sons, 2001.

[2] "Interface specification IS-GPS-200E," Global Positioning System Wing, Tech. Rep., Jun. 2010.

[3] K. Borre, D. M. Akos, N. Bertelsen, P. Rinder, and S. H. Jensen, *A Software-Defined GPS and Galileo Receiver: A Single Frequency Approach*. Birkhäuser, 2007.

[4] P. Ward, "GPS receiver search techniques," in *Proc. IEEE Position Location and Navigation Sym. (PLANS)*, Atlanta, Apr. 1996, pp. 604–611.

[5] E. D. Kaplan and C. J. Hegarty, Eds., *Understanding GPS: Principles and Applications*, 2nd ed. Artech House, 2006.

[6] C. O'Driscoll, M. G. Petovello, and G. Lachapelle, "Software receiver strategies for the acquisition and re-acquisition of weak GPS signals," in *ION National Tech. Meeting*, San Diego, Jan. 2008.

[7] A. Polydoros and C. Weber, "A unified approach to serial search spread-spectrum code acquisition–part I: General theory," *IEEE Trans. Commun.*, vol. 32, no. 5, pp. 542–549, May 1984.

[8] ——, "A unified approach to serial search spread-spectrum code acquisition–part II: A matched-filter receiver," *IEEE Trans. Commun.*, vol. 32, no. 5, pp. 550–560, May 1984.

[9] U. Cheng, W. J. Hurd, and J. I. Statman, "Spread-spectrum code acquisition in the presence of Doppler shift and data modulation," *IEEE Trans. Commun.*, vol. 38, no. 2, pp. 241–250, Feb. 1990.

[10] J. H. J. Iinatti, "On the threshold setting principles in code acquisition of DS-SS signals," *IEEE J. Sel. Areas Commun.*, vol. 18, no. 1, pp. 62–72, Jan. 2000.

[11] G. E. Corazza, "On the MAX/TC criterion for code acquisition and its application to DS-SSMA systems," *IEEE Trans. Commun.*, vol. 44, no. 9, pp. 1173–1182, Sep. 1996.

[12] D. Borio, L. Camoriano, and L. Lo Presti, "Impact of GPS acquisition strategy on decision probabilities," *IEEE Trans. Aerosp. Electron. Syst.*, vol. 44, no. 3, pp. 996–1011, Jul. 2008.

[13] D. Borio, C. O'Driscoll, and G. Lachapelle, "Coherent, non-coherent and differentially coherent combining techniques for the acquisition of new composite GNSS signals," *IEEE Trans. Aerosp. Electron. Syst.*, vol. 45, no. 3, pp. 1227–1240, Jul. 2009.

[14] C. O'Driscoll and C. C. Murphy, "Performance analysis of an FFT based fast acquisition GPS receiver," in *ION National Tech. Meeting*, San Diego, Jan. 2005, pp. 1014–1025.

[15] A. Lapidoth, *A Foundation in Digital Communication*. Cambridge: Cambridge University Press, 2009.

[16] S. U. Qaisar and A. Dempster, "Cross-correlation performance comparison of L1 & L2C GPS codes for weak signal acquisition," in *Proc. Int. Sym. on GPS/GNSS*, Nov. 2008.

[17] D. M. Akos, P.-L. Normark, J.-T. Lee, and K. G. Gromov, "Low power global navigation satellite system (GNSS) signal detection and processing," in *Proc. ION GPS*, Sep. 2000, pp. 784–791.

[18] B. W. Parkinson and J. J. Spilker, *Global Positioning System: Theory and Applications, Volume I*. Progress in Astronautics and Aeronautics, 1996, vol. 163.

[19] M. Soudan and B. C. Geiger, "On the averaging correlation for satellite acquisition in software defined radio receivers," in *Proc. ION GNSS*, Portland, Sep. 2010, pp. 3284–3289.

[20] J. A. Starzyk and Z. Zhu, "Averaging correlation for C/A code acquisition and tracking in frequency domain," in *Proc. IEEE Midwest Sym. on Circuits and Systems (MWSCAS)*, vol. 2, Dayton, Aug. 2001, pp. 905–908.

[21] M. Fantino, A. Molino, and M. Nicola, "An acquisition strategy suitable for software GNSS receivers," in *Proc. European Navigation Conference - Global Navigation Satellite Systems (ENC-GNSS)*, May 2009.

[22] M. Abramowitz and I. A. Stegun, Eds., *Handbook of Mathematical Functions with Formulas, Graphs, and Mathematical Tables*, 9th ed. Dover Publications, 1972.

[23] J. Jung, "Receiver having a ratio-based signal acquisition method," Sunnyvale, Jan. 2007.

[24] ——, "Implementation of correlation power peak ratio based signal detection method," in *Proc. ION GNSS*, Long Beach, Sep. 2004, pp. 486–490.

[25] B. C. Geiger, M. Soudan, and C. Vogel, "On the detection probability of parallel code phase search algorithms in GPS receivers," in *Proc. IEEE Int. Sym. on Personal, Indoor and Mobile Radio Communications (PIMRC)*, Istanbul, Sep. 2010, pp. 864–869.

[26] B. C. Geiger, C. Vogel, and M. Soudan, "A comparison of GNSS acquisition strategies," submitted to IEEE Trans. Aerosp. Electron. Syst.

[27] J. I. Marcum, "A statistical theory of target detection by pulsed radar," *IRE Transactions on Information Theory*, vol. 6, pp. 59–144, Apr. 1960.

[28] D. A. Shnidman, "The calculation of the probability of detection and the generalized marcum q-function," *IEEE Trans. Inf. Theory*, vol. 35, no. 2, pp. 389–400, March 1989.

[29] A. Papoulis and U. S. Pillai, *Probability, Random Variables and Stochastic Processes*, 4th ed. New York, NY: McGraw Hill, 2002.